ORIGINAL ARTICLE

Targeting toll-like receptor 7 as a therapeutic development strategy for systemic lupus erythematosus

Meng Wang[d,†], Hekai Chen[a,†], Tuan Zhang[a,†], Zhikuan Zhang[b,†], Xuwen Xiang[d], Meng Gao[d], Yilan Guo[d], Shuangshuang Jiang[a], Kejun Yin[a], Mintao Chen[a], Jian Huang[a,‡], Xincheng Zhong[a], Umeharu Ohto[b], Jing Li[c], Toshiyuki Shimizu[b,*], Hang Yin[a,*]

[a]State Key Laboratory of Membrane Biology, School of Pharmaceutical Sciences, Tsinghua-Peking Center for Life Sciences, Key Laboratory of Bioorganic Phosphorous Chemistry and Chemical Biology (Ministry of Education), Tsinghua University, Beijing 100084, China
[b]Graduate School of Pharmaceutical Sciences, the University of Tokyo, Tokyo 113-0033, Japan
[c]Department of Rheumatology and Clinical Immunology, Peking Union Medical College Hospital, Chinese Academy of Medical Sciences, Peking Union Medical College, Beijing 100032, China
[d]Toll Biotech Co., Ltd. (Beijing), Beijing 102209, China

Abstract Endosomal TLRs (TLR3/7/8/9) are highly analogous innate immunity sensors for various viral or bacterial RNA/DNA molecular patterns. Among them, TLR7, in particular, has been suggested to be a target for various inflammatory disorders and autoimmune diseases including systemic lupus erythematosus (SLE); but few small-molecule inhibitors with elaborated mechanism have been reported in literature. Here, we reported a well-characterized human TLR7-specific small-molecule inhibitor, TH-407b, with promising potency and negligible cytotoxicity through a novel binding mechanism. Notably, TH-407b not only effectively inhibited TLR7-mediated pro-inflammatory signaling in a variety of cultured cell lines but also demonstrated potent inflammation suppressing activities in primary peripheral blood mononuclear cells (PBMCs) derived from SLE patients. Furthermore, TH-407b showed prominent

*Corresponding authors.
  E-mail addresses: shimizu@mol.f.u-tokyo.ac.jp (Toshiyuki Shimizu), yin_hang@tsinghua.edu.cn (Hang Yin).
†These authors made equal contributions to this work.
‡Current address: Institute of Bio-Architecture and Bio-Interactions (IBABI), Shenzhen Medical Academy of Research and Translation, Shenzhen 518107, China

efficacy *in vivo*, improved survival rate and ameliorated symptoms of SLE model mice. To obtain molecular insights into the TH-407b derivatives' inhibition mechanism, we performed the structural analysis of TLR7/TH-407b complex using cryogenic electron microscopy (cryo-EM) method. As an atomistic resolution cryo-EM structure of the TLR family, it not only of value to facilitate structure-based drug design, but also shed light to methodology development of small proteins using EM. Significantly, TH-407b has unveiled an inhibition strategy for TLR7 *via* stabilizing its resting/inactivated state. Such a resting state could be generally applicable to all TLRs, rendering a useful method for targeting this group of important immunological receptors.

1. Introduction

Toll-like receptors (TLRs) are pattern recognition receptors (PRRs), recognizing pathogen-associated molecular patterns (PAMPs) and thereby regulating the immune responses[1,2]. Dysregulation of TLRs signaling contributes to the development and progression of numerous diseases such as rheumatoid arthritis[3] and systemic lupus erythematosus[4,5]. Therefore, TLRs are emerging as important drug targets[6] for autoimmune diseases. Traditionally, it was believed that PAMP molecules triggered pro-inflammatory signaling cascades through TLRs dimerization. However, the activation mechanism of endosomal TLRs remained elusive. Take TLR8 as an example, an unliganded dimer, particularly designated as the resting state, had been suggested to preform before the recognition of PAMP molecules. As a paradigm-shifting study, our group reported selective TLR8 inhibitors that stabilizing the resting state[7-9], thus interrupting the downstream signaling process. Nonetheless, there was little understanding whether this mechanism also applied to other endosomal TLRs. Among the endosomal TLRs, TLR7 and TLR8 show high sequence and function similarities[1,2], but few selective inhibitors with elaborated inhibition mechanism have been reported for TLR7, primarily attributed to the challenges of structural analysis for the TLR7-inhibitor complexes[10,11]. Thus, we set out to test the hypothesis that "stabilizing the resting state" could be generally applicable to other endosomal TLRs, in particular TLR7, a highly relevant target for therapeutic development.

Systemic lupus erythematosus (SLE) is an autoimmune disease that most often diagnosed in women at age of 20−40 (with a female to male ratio of 7:1−9:1)[12,13]. Exhibiting characteristics of a multisystem ailment, SLE was characterized by a multifaceted etiopathogenesis. The abnormal activation of TLR7 was previously considered to be associated with SLE, but the mechanism has not been clearly clarified at present[14-17]. In 2022, the clinical trial application for *enpatoran* (M5049), a TLR7/8 co-inhibitor developed by Merck, was approved by the Drug Administration for the treatment of SLE[18]. Our previous study also showed that TLR7 selective inhibitors could improve the survival rate and relieve renal injury of lupus prone mice[19]. In this study, we report a proof-of-concept that TLR7 inhibitors demonstrate therapeutic potential in the treatment of SLE, which was supported by *in vitro* experiments of patients' peripheral blood mononuclear cells (PBMCs) and *in vivo* studies of SLE animal models.

2. Materials and methods

2.1. Tests in human specimens

Human whole blood was collected by venipuncture from systemic lupus erythematosus (SLE) patients and healthy human volunteers as contrast. All experiments performed on human PBMCs have been described and approved by the IRB of PUMCH (No. S-478) and are consistent with Institutional Guidelines. Human PBMCs from three SLE patients were isolated using density gradient centrifugation. Immediately after separation, cells were cultured at a density of 3×10^6 cells/mL in 0.2 mL of RPMI 1640 in 96-well round-bottom plates (Thermo Scientific). Cells were then treated with indicated compound TH-407b. After incubating for 24 h, the supernatants were collected after centrifuged for 10 min at 4000 rpm at 4 °C and frozen at −80 °C until ready for Elisa measurements. The levels of TNF-α, IL-6 and IL-1β were determined using BD OptEIATM human TNF, IL-6 and IL-1β-ELISA kit (BD Biosciences) according to the manufacturer's instructions[8,9].

2.2. MRL/lpr mice model

Fourteen-week-old female MRL/lpr mice were used in this study. At the initiation of treatment, mice were randomly allocated into groups based on their body weight.

For verifying *in vivo* therapeutic potential of TH-407b, oral administration of the test substances was carried out either once or twice daily. The mice were divided into three groups ($n = 12$ per group) as follows: the treated group received oral administration of TH-407b at a dose of 100 mg/kg, dissolved in a 10% *w/v* solution of polyethylene glycol 400 (PEG-400) and 1,3-propanediol in water (55:20:25); the positive control group received daily oral administration of hydroxychloroquine (HCQ) at a dose of 100 mg/kg, dissolved in saline; and the placebo group received oral administration of saline in an equivalent volume. Throughout the treatment period, mice were anesthetized using isoflurane and blood samples were collected weekly *via* the fundus vein. The mice's survival, body weight, and severity of skin lesions were monitored on a weekly basis. After four weeks of treatment, the mice were euthanized, and their bodies were dissected. Spleen weight was measured as part of the analysis. Both kidneys were fixed in 10% neutral-buffered formalin, embedded in paraffin, sectioned, stained with hematoxylin and eosin (HE), and subsequently examined using light microscopy.

For verifying *in vivo* therapeutic potential of **S14**, oral administration of the test substances was carried out either once daily. The mice were divided into three groups ($n = 12$ per group) as follows: the treated group received oral administration of **S14** at a dose of 50 mg/kg, dissolved in a 10% *w/v* solution of poly-ethylene glycol 400 (PEG-400) and 1,3-propanediol in water (55:20:25); and the placebo group received oral administration of saline in an equivalent volume. Throughout the treatment period, mice were anesthetized using isoflurane and blood samples were collected weekly *via* the fundus vein. The mice's survival, body weight, and severity of skin lesions were monitored on a weekly basis. After four weeks of treatment, the mice were euthanized, and their bodies were dissected. Spleen weight was measured as part of the analysis. Both kidneys were fixed in 10% neutral-buffered formalin, embedded in paraffin, sectioned, stained with hematoxylin and eosin (HE), and subsequently examined using light microscopy.

2.3. High-throughput screening (HTS)

HEK-Blue hTLR7 cells were purchased from Invitrogen (cat. hkb-htlr7), which can stably express human TLR7 and a secreted embryonic alkaline phosphatase (SEAP) reporter. More than one hundred thousand of small-molecule compounds from Chembridge library, Sigma drug library and Selleck library were screened in 384-well plates at the platform of School of Pharmaceutical Sciences, Tsinghua University using SEAP assay we had reported previously. The initial concentration of small-molecule compounds was 5 μmol/L. A promising hit compound (Sigma-5-8-L20) from Sigma library was successfully obtained.

2.4. SEAP reporter assay

HEK-Blue TLR7 cells were plated at 5×10^5 cells/mL in a tissue culture treated 96-well plate in dulbecco's modified eagle medium (DMEM) with 10% (*v/v*) fetal bovine serum (FBS) (deactivated phosphatases). Then cells were treated with 2 μg/mL R848 (Invivogen) and varying concentrations of appropriate compounds. Cells were incubated with compounds and R848 at 37 °C. After incubation for 20−24 h, 50 μL culture media was taken out and placed in a new 96-well plate. 50 μL Quanti-Blue (Invivogen) was added to the media, and the plate was incubated at 37 °C until color changed obviously (about 30 min). The plates were then quantified on a Beckman−Coulter DTX 880 Multimode Detector by measuring absorbance at 620 nm. Data was normalized as readout of R848-treated cells is 100% activation, and untreated cells are 0% activation[7,8].

2.5. Cell viability assay

HEK-Blue TLR7 cells (5×10^5 cells/well) or human PBMCs (3×10^6 cells/mL) were placed in a 96-well plate and co-incubated with indicated compounds at 37 °C for 24 h. Then Cell Counting Kit-8 (Bimake) was added to each well (1:10 dilution). Then, the cells were incubated at 37 °C until a color change was observed (within 2 h) and absorbance was read at 450 nm. Data were normalized with the untreated cells control as 100% survival.

2.6. RT-PCR analysis of IL-8 mRNA expression

HEK-Blue TLR7 cells were seeded at a density of 1×10^6 cells/well in a 6-well plate. After 24 h incubation, the medium was replaced by serum free medium, and then the cells were treated with or without R848 (2 μg/mL) and various concentrations of compound for 16 h at 37 °C. Then, cells were scraped and re-suspended in phosphate buffer saline (PBS). Total RNA was extracted using Trizol reagent (Invitrogen, No. 15596026) with standard protocols. Reverse transcription was performed by iScript™ cDNA Synthesis Kit (Bio-rad, No. 1708890) according to manufacturer's instructions. qPCR was performed using iTaq Universal SYBR Green Supermix (Bio-Rad, No. 1725120). IL-8 and GAPDH primers were obtained from Ruibiotech. Data were analyzed using the ΔΔCt method with GAPDH gene as a housekeeping gene, normalized to cells control.

2.7. RT-PCR analysis of IFN-α and ISGs mRNA expression

Human blood was drawn from healthy donors into vacutainer tubes with EDTA as the anticoagulant and used within 2 h of collection. Two volumes of blood were diluted with one volume of PBS, and 1.5 mL per well of the diluted blood was dispensed per well of 12-well plates. The cells were treated with R848 (5 μg/mL) and various concentrations of compound for 24 h at 37 °C. Total RNA was extracted using Trizol reagent (invitrogen, No. 15596026) with standard protocols. Reverse transcription was performed by iScript™ cDNA Synthesis Kit (Bio-rad, No. 1708890) according to manufacturer's instructions. qPCR was performed using iTaq Universal SYBR Green Supermix (Bio-Rad, No. 1725120).

GAPDH forward primers: 5′-CATGAGAAGTATGACAACAGCCT-3′

GAPDH reverse primers: 5′-AGTCCTTCCACGATACCAAAGT-3′

IFN-α forward primers: 5′-GCCTCGCCCTTTGCTTTACT-3′
IFN-α reverse primers: 5′-CTGTGGGTCTCAGGGAGATCA-3′
IRF7 forward primers: 5′-AAGAGCCTGGTCCTGGTGAA-3′
IRF7 reverse primers: 5′-TCGATGTCGTCATAGAGGCTGTT-3′
IFI6 forward primers: 5′-GGTCTGCGATCCTGAATGGG-3′
IFI6 reverse primers: 5′-TCACTATCGAGATACTTGTGGGT-3′
IFI27 forward primers: 5′-CTTCACTGCGGCGGGAATC-3′
IFI27 reverse primers: 5′-CCAGGATGAACTTGGTCAATCC-3′
IFI44 forward primers: 5′-TGGTACATGTGGCTTTGCTC-3′
IFI44 reverse primers: 5′-CCACCGAGATGTCAGAAAGAG-3′
IFI44L forward primers: 5′-AAGTGGATGATTGCAGTGAG-3′
IFI44L reverse primers: 5′-CTCAATTGCACCAGTTTCCT-3′

Data were analyzed using the ΔΔCt method with *GAPDH* gene as a housekeeping gene, normalized to cells control.

2.8. Enzyme-linked immunosorbent assay (ELISA)

ELISA was performed to measure TNF-α and IL-6 expression levels. Raw 264.7 cells seeded at 2×10^6 cells/well in 2 mL supplemented Roswell Park Memorial Institute (RPMI) medium [10% (*v/v*) FBS, 2 mmol/L L-glutamine, 100 μg/mL streptomycin

and 100 U/mL penicillin and 0.05 mmol/L 2-mercaptoethanol] in 6-well plates and incubated at 37 °C in a humidified 5% CO_2 atmosphere. After 24 h, the medium was replaced with un-supplemented RPMI medium, and the cells were treated with or without R848 (2 μg/mL) and various concentrations of com-pounds. After 24 h, supernatants of the culture media were collected, and the levels of TNF-α and IL-6 were determined using mouse TNF-α and IL-6 OptEIA ELISA kit (BD Bio-sciences), according to the manufacturer's instructions[8,9].

Another ELISA was performed to measure ANA and anti ds-DNA antibodies levels. Blood was collected from eyeground venous plexus and plasma was collect by centrifugation (3000 rpm, 15 min, 4 °C). ANA and anti ds-DNA antibodies levels were determined using mouse ANA and anti-ds-DNA antibodies ELISA kit (Jiangsu Meibiao Biotechnology Co., Ltd.), according to the same instruction.

2.9. Western blot

Western blot analysis was performed in Raw 264.7 cells treated with 2 μg/mL R848 and TH-407b or THP-1 cells treated with 1 μg/mL TL8-506 and TH-407b to determine the upregulation/inhibition of TNF receptor associated factor 3 (TRAF3), phosphorylated-IKK (p-IKK) and IKK. Raw 264.7 or THP-1 cells were collected and lysed. Total protein was fractionated into cell lysis buffer (50 mmol/L Tris-HCl, 150 mmol/L NaCl, 10% glyc-erin, 0.2% Triton X-100, protease inhibitor 1 X, constant volume of Milli-Q pure water to 1 L and adjust pH to 7.5). Protein con-centrations were measured by Bradford assay and loaded into 10% Tris-glycine SDS-PAGE. Protein was transferred onto a PVDF Transfer membrane (Merck Millipore) by electroblotting (100 mA for 1 h) and probed with the primary antibody TRAF3 (CST; 4729), IKBα (Bioss; 1287R), p-IKBα (Bioss; 52169R) (1:1000). Then Peroxidase-conjugated AffiniPure Goat Anti-Rabbit IgG (H + L) antibody (for TRAF3, IKBα and p-IKBα) (CST) at 1:5000 dilution was used as secondary antibody. 5% w/v BSA in TBST was used for blocking the membrane, and primary, sec-ondary antibody preparation steps. Visualization of the blots was performed by Thermo SuperSignal West Pico kit (Thermo Fisher Scientific). GAPDH (CST; 2118) was used as internal controls for cytoplasmic fractions.

2.10. Protein expression and purification

Monkey (*Macaca mulatta*) TLR7 extracellular domain expression construct with N167Q, N399Q, N488Q, and N799Q mutations and cleavable Z-loop and C-terminal protein A tag described previously[21] were expressed in *Drosophila* S2 cells. Culture su-pernatant was purified using IgG Sepharose (GE Healthcare). The Z-loop and the protein A tag were then cleaved using thrombin protease (Nacalai tesque). The proteins were purified by gel-filtration chromatography using a HiLoad 26/600 Superdex 200 pg column (GE Healthcare) equilibrated in a buffer of 10 mmol/L HEPES-NaOH, pH 7.5, 150 mmol/L NaCl. Fractions were pooled, concentrated to ∼10−15 mg/mL, flashed cooled in liquid nitrogen, and kept at −70 °C until use. Glycan-trimmed TLR7 proteins were expressed in the presence of 1.5 mg/L kifu-nensine (Glycosyn) and treated by Endo Hf (New England Bio-labs). Glycan-untrimmed proteins were used in ITC analysis, crosslinking assay. Glycan-trimmed TLR7 proteins with partially-uncleaved protein A tag were used for cryo-EM analysis.

2.11. ITC titration

ITC experiments of TH-407b to TLR7 recombinant proteins were conducted at 298 K in a final buffer condition of 40 mmol/L citrate/NaOH pH 4.8 (Hampton Research), 150 mmol/L NaCl by using a MicroCal iTC200 (Malvern Panalytical). A solution containing 1 mmol/L TH-407b was titrated into a solution con-taining 80 μmol/L TLR7 protein, using a titration sequence of a single 0.4 μL injection followed by 18 injections, 2 μL each, with 180 s intervals between injections.

ITC experiments of loxoribine into TLR7 recombinant proteins in the absence or presence of 500 μmol/L TH-407b were con-ducted at 298 K in a final buffer condition of 30 mmol/L citrate/NaOH pH 4.8 (Hampton Research), 150 mmol/L NaCl by using a MicroCal iTC200 (Malvern Panalytical). A solution containing 1 mmol/L Loxoribine (Invivogen) was titrated into a solution containing 50 μmol/L TLR7 protein with or without 500 μmol/L TH-407b, using a titration sequence of a single 0.4 μL injection followed by 18 injections, 2 μL each, with 180 s intervals between injections.

OriginLab software (OriginLab) was used to analyze the raw ITC data. Thermodynamic parameters were extracted from curve fitting analysis with a single-site binding model.

ITC experiments of TH-407b to TLR7 recombinant proteins in the presence of loxoribine were conducted at 298 K in a final buffer condition of 40 mmol/L citrate/NaOH pH 4.8 (Hampton Research), 150 mmol/L NaCl by using a MicroCal iTC200 (Malvern Panalytical). A solution containing 1 mmol/L TH-407b was titrated into a solution containing 80 μmol/L TLR7 protein in the absence or presence of 100 μmol/L loxoribine, using a titration sequence of a single 0.4 μL injection followed by 18 injections, 2 μL each, with 180 s intervals between injections.

2.12. Crosslinking assay

For crosslinking assay using glutaraldehyde reagent (Nacalai tesque), TLR7 protein was adjusted to a final concentration of 25 μmol/L using buffers containing 50 mmol/L citrate/NaOH pH 4.8, 1507 mmol/L NaCl. GS9620, TH-407a, and TH-407b dis-solved in DMSO were added to final concentrations of 0.2 or 1.0 mmol/L. For TH-407a, due to its low solubility, it precipitated and could not reach a concentration of 1.0 mmol/L. The reactions were started by adding glutaraldehyde (Nacalai tesque) to a final concentration of 20 mmol/L, incubated at 20 °C for 30 min, and quenched by adding Glycine-HCl pH 5.0 to a final concentration of 100 mmol/L. Crosslinked samples were analyzed by non-reducing SDS-PAGE. Image-J software was used to perform a quantitative analysis of the SDS-PAGE gel image.

Crosslinked samples were also analyzed with a Superdex 200 Increase 10/300 GL column equilibrated in a buffer of 10 mmol/L citrate/NaOH pH 4.8, 100 mmol/L NaCl. The crosslinking con-dition was the same as above. About 60 μg crosslinked proteins in the absence or presence of 1.0 mmol/L TH-407b during the crosslinking reaction were injected into the column. UV absor-bance at 280 nm (A_{280}) and 260 nm (A_{260}) of the elutes were monitored.

2.13. Cryo-EM grid preparation and data collection

Crosslinked TLR7/TH-407b complex for cryo-EM analysis was prepared as follows: 30 μmol/L glycan-trimmed TLR7 with partially-uncleaved protein A tag, 1 mmol/L TH-407b, and

20 mmol/L glutaraldehyde were mixed in 50 mmol/L citrate/NaOH pH 4.7, 150 mmol/LNaCl buffer and reacted at 20 °C for 25 min. The reaction was quenched by adding glycine/HCl pH 5.0 to a final concentration of 100 mmol/L and incubated at 4 °C for 30 min. The sample was then purified with a Superdex 200 Increase 10/300 GL column equilibrated in a buffer of 10 mmol/L citrate/NaOH pH 4.8, 100 mmol/L NaCl. The dimer fractions were pooled and concentrated to ∼2.6 mg/mL using Amicon Ultra devices (Merck). The concentrated sample was diluted to ∼0.8 mg/mL using a buffer containing 10 mmol/L Citrate pH 4.8, 100 mmol/L NaCl, and 150 μmol/L TH-407b. A 3 μL aliquot of TLR7/TH-407b complex was applied to a glow-discharged Quantifoil grid (R1.2/R1.3 300 mesh, copper), blotted for 4 s in 100% humidity at 6 °C, and plunged into liquid ethane using a Vitrobot Mark IV (Thermo Fisher Scientific). Movie stacks were collected by using a Titan Krios G3i microscope (Thermo Fisher Scientific) at 300 kV equipped with a Gatan Quantum-LS Imaging Filter (GIF) and a Gatan K3 direct electron detector in the electron counting mode at the Cryo-EM facility in the University of Tokyo (Tokyo, Japan). Movie stacks were acquired using 105,000 × magnification with an accumulated dose of 57.9 electrons per Å[29] over 60 frames. The pixel size was 0.83 Å. The data were automatically acquired by the beam-image shift method using the SerialEM software[26].

2.14. Cryo-EM data processing and model building

Cryo-EM data processing was performed using RELION 3.0.6[27]. Raw movie stacks were motion-corrected using MotionCor2[28]. The CTF parameters were determined using the CTFFIND4 program[29]. The data processing workflow is summarized in Supporting Information Fig. S4. Briefly, bad micrographs were excluded based on CtfMaxResolution >5 Å. Particles were firstly picked from randomly selected 100 micrographs using the LoG-based auto-picking algorithm. Several rounds of 2D classification were performed and the 2D class average images were used as the templates for reference-based auto-picking which generated 3,211,637 particles. All particles were sub-divided into six subsets and two rounds of 2D classification were performed against each subset. Particles belonging to good class images were selected and merged. Then, a total of three rounds of 3D classification were performed and generated a particle package containing 337,415 particles. This particle package yielded an overall resolution of 3.2 Å. The final resolution was estimated by gold-standard Fourier shell correlation (FSC) between the two independently refined half maps (FSC = 0.143). The local resolution map was produced with the ResMap program[30]. For model building against the EM map, coordinates of two TLR7 monomers (PDB ID: 5GMH) were docked into the final map using Phenix dock in map program[31]. The model was then manually refined and built using the COOT program[32]. Real-space refinement in Phenix program was performed after manual refinement[31].

The cryo-EM map has been deposited in the Electron Microscopy Data Bank. The atomic coordinate of the TLR7/TH-407b complex structure has been deposited in the Protein Data Bank. The statistics of EM data processing and refinement were summarized in Supporting Information Table S1. Structure representations were generated in the Chimera[33], Pymol, and COOT programs[32].

2.15. Histopathological analysis

The both kidneys were fixed in 10% neutral-buffered formalin, embedded in paraffin, sectioned, stained with hematoxylin and eosin (HE) and periodic acid-Schiff (PAS), and examined by light microscopy (Zeiss, Axio Scan. Z1).

2.16. Pharmacokinetic profiling

Male ICR mice ($n = 12$, weighing 25 ± 3 g) were randomly assigned to two groups, namely the intravenous (iv) and oral administration groups, after an overnight fasting period. TH-407b or **S15** was dissolved in a mixture solution containing 5% dimethylacetamide (DMAC), 10% Solutol, and 85% saline for both intravenous and oral administration routes. The dose volume for both routes of administration was 10 mL/kg. In the first group, mice were administered a single intravenous tail vein bolus dose of 1 mg/kg TH-407b or **S15**, while in the second group, mice were given single oral doses of 5 mg/kg TH-407b or **S15**. Blood samples were collected from mice into heparinized tubes at specific time points, including 0.0833, 0.25, 0.5, 1, 2, 4, 6, 8, and 24 h following intravenous administration or 0.25, 0.5, 1, 2, 4, 6, 8, and 24 h after oral administration. Subsequently, plasma samples were obtained by centrifuging the blood samples at 10,000×g for 5 min at 4 °C in preparation for further analysis.

2.17. Acute toxicity assessment

TH-407b was orally administered to 14-week-old male and female C57BL/6 mice at 0, 100, 200, 400, 800, 1000 mg/kg dissolved in 0−10% w/v solution (PEG-400:1,3-propanediol:H_2O = 55:20:25), and saline was administered for the placebo group. Survival and body weight of the mice was measured within 7 days. Then the mice were euthanized and dissected, and heart, liver, spleen, kidney and lung were extracted and observed. The results showed that all the mice survived, and there was no significant difference in body weight among 7 groups, and there was no significant pathological change in the organs.

2.18. Long-term toxicity assessment

TH-407b dissolved in 0−10% w/v solution (PEG-400:1,3-propanediol:H_2O = 55:20:25), was orally administered to 14-week-old male and female C57BL/6 mice at 100 mg/kg twice daily. And saline was administered for the placebo group. Survival and body weight of the mice was measured within 28 days. Then the mice were euthanized and dissected, and heart, liver, spleen, kidney and lung were extracted and observed. The results showed that all the mice survived, and there was no significant difference in body weight among 2 groups, and there was no significant pathological change in the organs.

3. Results

### 3.1. Identification of potent and selective TLR7 inhibitors

To discover potential specific TLR7 inhibitors, we firstly performed a preciously-established cell-based high-throughput screening assay using engineered HEK-Blue 293 cell lines stably overexpressing different human TLRs. The TLRs-mediated nuclear factor kappa-B (NF-κB) activation could be tested by measuring the secreted embryonic alkaline phosphatase (SEAP) activity. Several commercial small molecule libraries, which contained more than 100,000 drug-like compounds, were screened, and the 5-(piperazin-1-yl) quinoline derivative **S1** was
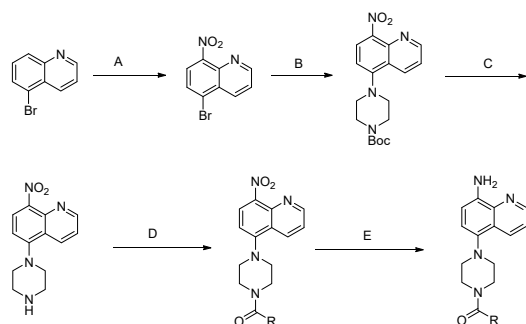
Scheme 1 Synthesis of compounds **S1−S14**, **S18−S19**, **S21−S30**. Reagents and conditions: (A) H_2SO_4, HNO_3, r.t., 3 h; (B) 1-Boc-piperazine, K_2CO_3, DMF, reflux, 18 h; (C) TFA, DCM, 30 °C, 2 h; (D) Et_3N, DCM, r.t., 6 h; (E) Fe/HCl, rt, overnight.

identified as potential TLR7/8 dual inhibitor with no obvious inhibition to other homologous TLRs (TLR1/2/6, TLR3, TLR4, TLR5, and TLR9) (Supporting Information Fig. S1A).

To obtain a more potent and specific small-molecule inhibitor for TLR7, we developed a concise synthetic route for the 5-(piperazin-1-yl) quinoline scaffold for structural optimization. The representative synthetic route of the hit compound was shown in Schemes 1−4. The overall synthetic route of the other compounds was similar to hit compound **S1**. Details were slightly different, listed in Supporting Information. We divided the structure of the hit compound into three parts for detailed structure−activity relationship (SAR) studies and aimed for the potential selective inhibitor for TLR7. For part A, we tried different substituent modifications to the benzene ring. The results indicated that electron-donating group showed higher potency than that of electron-withdrawing group (**S2** vs **S3**), and the stronger the electron donating ability was (**S4** vs **S2**), the better inhibitory activity. Different positions of the methoxy group introduced to the benzene ring have been explored, and the para-substitution (**S4**) showed better activity than either meta- (**S9**) or ortho- (**S10**) modification, suggesting a particular orientation was desired. The multiple substituents (**S11**) did not obviously improved the inhibitory activity for TLR7. The replacement of the benzene ring by other five- or six-membered rings had no obvious impact on TLR7 inhibitory activity or selectivity (**S6** vs **S12** to **S14**). Therefore, the para-substituted methoxyphenyl group was chosen as the optimal one for part A for the following exploration. Then, we focused on part B and part C. We found that changing the intermediate linker resulted in the decreased TLR7 inhibitory activities (**S4** vs **S17**, **S18**). Thus, piperazine and carbonyl groups were still preferred for part B. Moreover, removing, replacing or changing the position of the nitrogen atom and nitro group in quinoline group
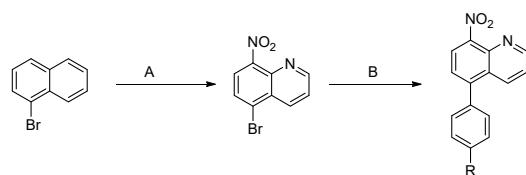
Scheme 2 Synthesis of compounds **S15** and **S16**. Reagents and conditions: (A) H_2SO_4, HNO_3, r.t., 3 h; (B) tetraphenylphosphine palladium (0), sodium carbonate, toluene, 90 °C, overnight.
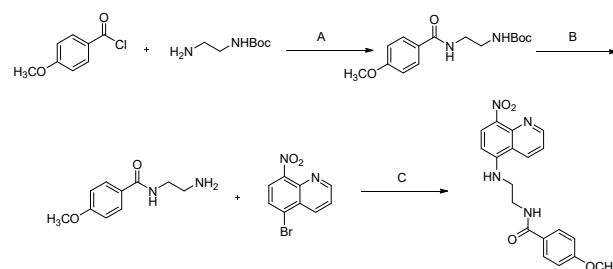
Scheme 3 Synthesis of compounds **S17**. Reagents and conditions: (A) Et_3N, DCM, r.t., 2.5 h; (B) TFA, DCM, r.t., overnight; (C) 4,5-bis(diphenylphosphino)-9,9-dimethylxanthene, cesium carbonate, tris(dibenzylideneacetone) dipalladium, toluene, 100 °C, overnight.

would decrease or even loss the activity to both TLR7 and TLR8 (**S1** vs **S20** and **S4** vs **S21** to **S26**) dramatically. Therefore, we kept these two parts in the following exploration. Finally, back to part A, we tried to replace benzene with a larger group. When the substituted benzene ring was replaced by adamantane (**S1** vs **S27**), the selectivity was significantly reversed. And with hydrophilic group in adamantane, the TLR7 inhibitory activity was obviously better than that of TLR8 (**S28**, **S30** vs **S29**). Among them, **S30** modified with carbonyl in adamantine showed the best activity and selectivity, which was designated as TH-407b.

Through the extensive structure−activity relationship (SAR) study (Table 1), we successfully obtained a specific TLR7 inhibitor TH-407b with improved potency and negligible cytotoxicity. The half maximal inhibitory concentration (IC_{50}) value of TH-407b in HEK-Blue hTLR7 cells is 0.23 ± 0.03 μmol/L, superior to the reported ones[10,11] (Fig. 1A).

3.2. TH-407b inhibited TLR7 signaling pathway and TLR7-mediated cytokine production

TLR7 activation initiates the signaling cascade and leads to the increased production of the pro-inflammatory cytokines such as tumor necrosis factor-α (TNF-α), interleukin-6 (IL-6) and interleukin-8 (IL-8)[20]. In order to confirm the on-target effect of TH-407b to TLR7 in the complex cellular environment, several experiments were performed to prove TH-407b indeed specifically inhibit the TLR7 downstream signaling in cultured cell lines.

First, we indicated the effect of TH-407b on inhibiting pro-inflammatory cytokine, IL-8, in mRNA level in HEK-Blue hTLR7 cells induced by R848, a known synthetic agonist for TLR7/8, through quantitative reverse transcription-polymerase chain reaction (RT-PCR) (Fig. 1B). We found that different concentrations of TH-407b could inhibit IL-8 mRNA levels in a dose-dependent manner with the inactive analog **S24** as a negative control.

Then, we conducted further assays to verify the inhibition of TH-407b to various cytokines. R848 treatment significantly increased TNF-α production after 24 h. While TH-407b could dose-dependently inhibit TNF-α and IL-6 production in 2 μg/mL R848 treated RAW 264.7 cells by ELISA (Fig. 1C).

Finally, we further confirmed that TH-407b targeted TLR7 by Western blot. TNF receptor associated factor 3 (TRAF3) and the phosphorylated NF-kappa-B inhibitor alpha (p-IKBα), are all important downstream proteins to TLR7[1,2]. When R848 was added to activate the TLR7 signaling pathway, TRAF3 and p-IKBα levels were increased. And we found that when the TH-407b was added, TRAF3 and p-IKBα were significantly inhibited (Fig. 1D and
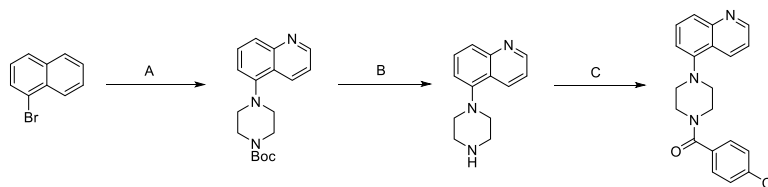
Scheme 4 Synthesis of compounds **S-20**. Reagents and conditions: (A) 1,1′-dinaphthalene-2,2′-didiphenylphosphine, *tert*-butanol sodium, tri (dibenzyl acetone) dipalladium, toluene, 100 °C, 12 h; (B) TFA, DCM, 30 °C, 2 h; (C) Et$_3$N, DCM, r.t., 6 h.
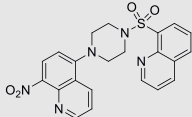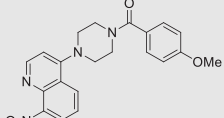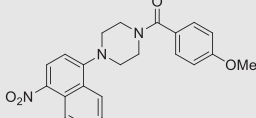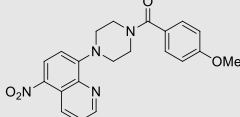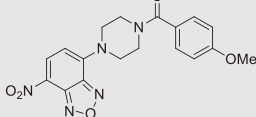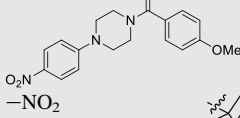
Table 1 Representative structure−activity relationship (SAR) results for inhibitory activities of 5-(piperazin-1-yl) quinoline derivatives in HEK-Blue hTLR7 and HEK-Blue hTLR8 cells.

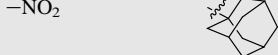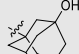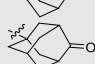| Compound	R$_1$	R$_2$	IC$_{50}$ (μmol/L)[a,b] (TLR7)	IC$_{50}$ (μmol/L)[a,b] (TLR8)
S1 (Hit)	−NO$_2$	4-Cl−C$_6$H$_4$−	0.79 ± 0.27	0.13 ± 0.03
S2	−NO$_2$	4-CH$_3$−C$_6$H$_4$−	0.86 ± 0.39	0.11 ± 0.04
S3	−NO$_2$	4-CF$_3$−C$_6$H$_4$−	1.90 ± 0.52	0.58 ± 0.11
S4	−NO$_2$	4-OCH$_3$−C$_6$H$_4$−	0.53 ± 0.09	0.07 ± 0.01
S5	−NO$_2$	4-NO$_2$−C$_6$H$_4$−	0.64 ± 0.21	0.15 ± 0.04
S6	−NO$_2$	C$_6$H$_5$−	1.07 ± 0.42	0.10 ± 0.07
S7	−NO$_2$	4-F−C$_6$H$_4$−	1.15 ± 0.16	0.10 ± 0.05
S8	−NO$_2$	4-Br−C$_6$H$_4$−	0.97 ± 1.23	0.14 ± 0.17
S9	−NO$_2$	3-OCH$_3$−C$_6$H$_4$−	1.28 ± 1.05	0.08 ± 0.03
S10	−NO$_2$	2-OCH$_3$−C$_6$H$_4$−	3.06 ± 2.72	0.06 ± 0.01
S11	−NO$_2$	2,4-diOCH$_3$−C$_6$H$_3$−	0.41 ± 0.33	0.06 ± 0.03
S12	−NO$_2$		2.12 ± 0.58	0.06 ± 0.03
S13	−NO$_2$		0.53 ± 0.11	0.10 ± 0.01
S14	−NO$_2$		3.00 ± 0.37	0.06 ± 0.01
S15			0.02 ± 0.01	0.02 ± 0.01
S16			0.66 ± 0.13	1.3 ± 0.03
S17			N.A.	N.A.
S18			1.14 ± 0.94	5.18 ± 0.67

(continued on next page)

Table 1 (*continued*)

Compound	R₁	R₂	IC₅₀ (μmol/L)[a,b] (TLR7)	IC₅₀ (μmol/L)[a,b] (TLR8)
S19			N.A.	N.A.
S20	—H	4-Cl—C₆H₄—	N.A.	N.A.
S21	—NH₂	4-OCH₃—C₆H₄—	N.A.	0.82 ± 0.04
S22			N.A.	N.A.
S23			N.A.	N.A.
S24			N.A.	N.A.
S25			N.A.	N.A.
S26			N.A.	N.A.
S27 (TH-407a)	—NO₂		0.47 ± 0.05	4.57 ± 0.76
S28	—NO₂		0.43 ± 0.09	1.47 ± 0.45
S29	—NO₂		2.62 ± 0.54	3.89 ± 0.78
S30 (TH-407b)	—NO₂		0.23 ± 0.03	1.26 ± 0.30

[a] IC₅₀ values and corresponding standard deviations were determined from at least three independent biological replicates.
[b] N.A. means no significant inhibitory activity at 100 μmol/L.

Supporting Information Fig. S13). We also assessed the TRAF and p-IKBα protein levels within THP-1 cells subsequent to TL8-506 stimulation. When TL8-506 was added to activate the TLR8 signaling pathway, TRAF3 and p-IKBα levels were increased. And we found that only the highest concentration of TH-407b was added, TRAF3 and p-IKBα were inhibited (Figs. S1B and S13).

3.3. TH-407b binds to TLR7 and induces receptors dimerization

To explore the inhibition mechanism, an ITC titration analysis was conducted to examine whether TH-407b directly binds to TLR7 extracellular domain. A TH-407b solution at 1 mmol/L concentration titrated to an 80 μmol/L TLR7 protein solution, and as a

result, the enthalpy change ($\Delta H = -7868$ cal/mol) confirmed the direct binding of TH-407b to TLR7 extracellular domain with a moderate binding affinity ($K_D = 5.1$ μmol/L) (Fig. 2A). The binding affinity of TH-407b is comparable to that of synthetic TLR7 agonists, such as loxoribine[21]. To further investigated the oligomerization state of TLR7 upon TH-407b binding, we performed a crosslinking assay using glutaraldehyde reagent and quantitatively investigated the band intensity (Fig. 2B). The results showed that part of TLR7 was crosslinked to dimers even in the absence of ligands, indicating that TLR7 might form an unliganded dimer in a similar manner with TLR8[22]. In the presence of a TLR7-specific agonist, GS9620, a large amount of TLR7 transformed to dimers, reconfirming that TLR7 forms a dimer
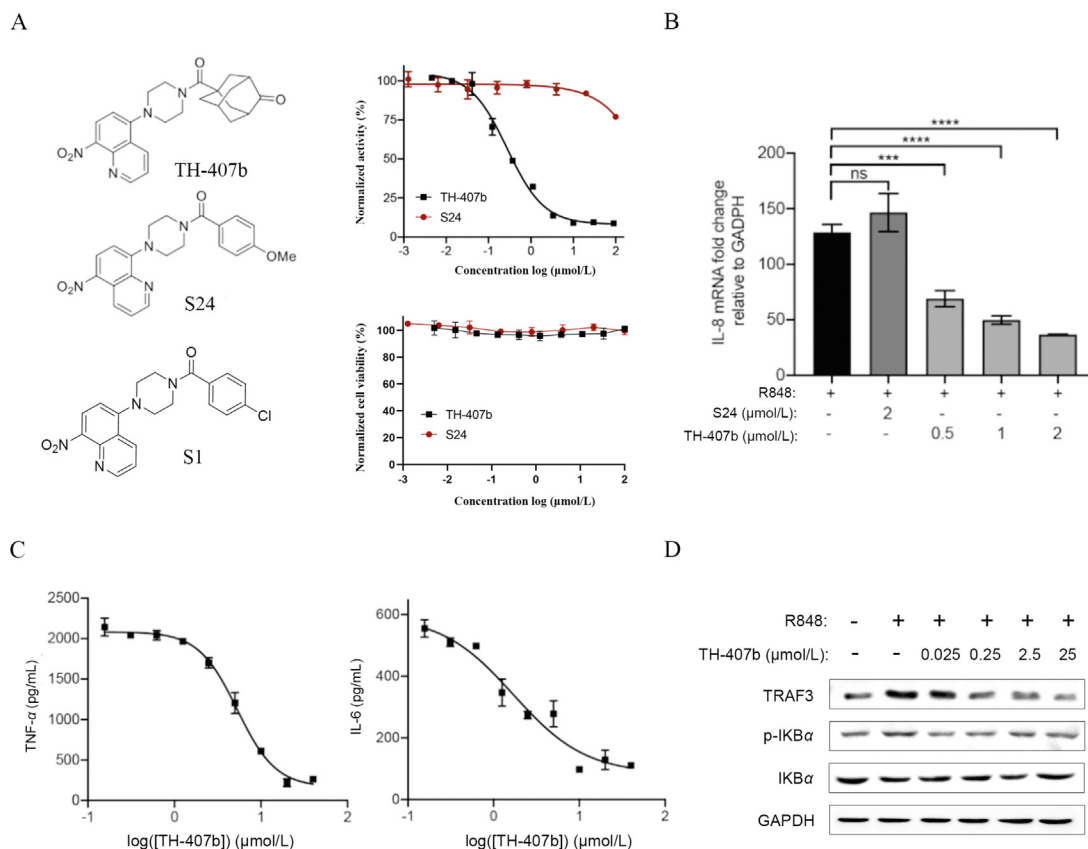
A

B

C

D

Figure 1 Characterizations of novel selective TLR7 inhibitor. (A) TH-407b dose-dependently inhibited R848-induced TLR7 activation with an IC_{50} of 0.23 ± 0.03 µmol/L, while its analog **S24** showed much lower potency. (B) IL-8 mRNA level in 2 µg/mL R848 treated HEK-Blue TLR7 cells under different concentrations of TH-407b with **S24** as a control. (C) TH-407b could dose-dependently inhibit TNF-α and IL-6 production in 2 µg/mL R848 treated RAW 264.7 cells by ELISA. (D) The expression of TRAF3 and p-IKBα in the TLR7 downstream signaling pathway could be inhibited by TH-407b. (Center lines indicate means, and whiskers indicate $\pm$ SEM. P values were determined using one-way ANOVA; ***$P < 0.001$, ****$P < 0.0001$).

when activated by agonistic ligand, which is consistent with the crystal structures of TLR7[21]. The novel antagonists, TH-407b and its derivative TH-407a also increased the TLR7 dimer proportion in a concentration-dependent manner, and the band shape of the antagonist-induced dimer was distinct from that of the GS9620-induced dimer, indicating a different pattern of crosslinking. Gel filtration analysis of crosslinked TLR7 samples also confirmed that TH-407b induced the formation of dimeric TLR7 (Fig. 2C). Therefore, we speculated that upon antagonist binding, TLR7 can form a distinct dimeric structure compared to the activated form.

3.4. Cryo-EM structure of TLR7/TH-407b complex

Next, we performed the cryo-EM analysis of the TLR7/TH-407b complex to visualize the recognition mechanism of TH-407b by TLR7. To prevent the dissociation of the complex, we utilized a crosslinked form of the TLR7/TH-407b complex (Supporting Information Fig. S2). We successfully determined the cryo-EM structure of this crosslinked TLR7/TH-407b complex at a 3.2 Å resolution (Fig. 3A and B, Supporting Information Fig. S3, and Table S1). The overall structure of the TLR7/TH-407b complex adopts a C2-symmetric open-form conformation formed by face to face interaction of two TLR7 protomers (TLR7 and TLR7*, throughout this paper, we use asterisks to indicate the second

TLR7 and its residues). The densities of TH-407b are clearly observed inside the TLR7 dimerization interface (Supporting Information Fig. S4). The C-termini of the two protomers are separated with a distance of 69 Å, preventing the subsequent assembly of the cytosolic signaling domain. Thus, we refer this TLR7/TH-407b complex structure as an inactivated conformation. In comparison to the activated TLR7 dimer (TLR7/GS9620 complex)[23], when the two structures are aligned according to one TLR7 protomer, the second TLR7* protomer exhibits a large displacement of 37 Å at their C-termini (Fig. 3C). When compared to the TLR8/CU-CPT8m complex structure[8], inactivated dimers of both TLR7 and TLR8 harbor separated C-terminus of the protomers, but those of the TLR7 is more separated from each other compared to those of TLR8. Actually, the dimerization interfaces of the TLR7/TH-407b complex and the TLR8/CU-CPT8m complex are spatially conserved and have either similar or different features of interaction (Supporting Information Fig. S5A and S5B).

The TH-407b binding site is composed of residues from LRR8, LRR11-13, and LRR15*-17*, which is spatially distinct from the agonist binding site of TLR7 (LRR8, LRR11-14 and LRR16*-18*) (Fig. 3D). TH-407b is recognized via characteristic hydrophobic and hydrogen bond interactions (Fig. 3E). Specifically, the TH-407b backbone is surrounded by a pocket composed of many
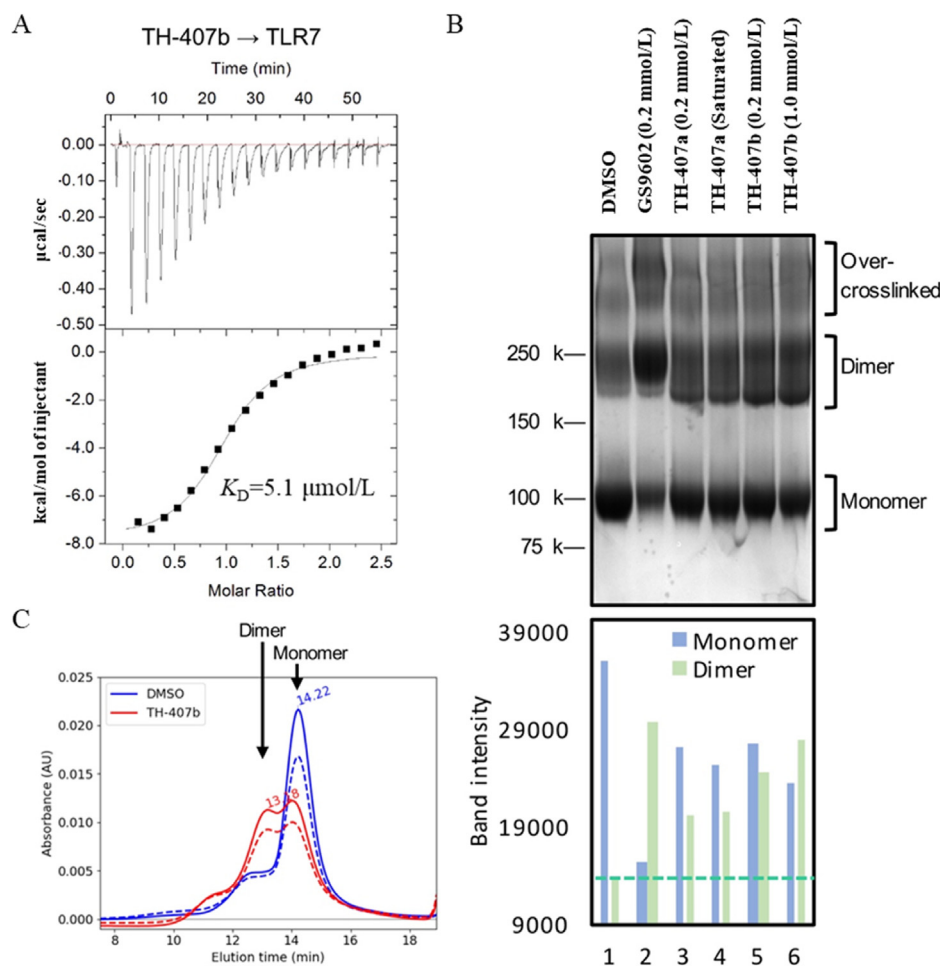
Figure 2 TH-407b binds to TLR7 and induces receptor dimerization. (A) ITC titration of TH-407b to TLR7 recombinant proteins. Dissociation constant value (K_D) is indicated. (B) Crosslinking assay of ligand-induced dimerization of TLR7. The non-reduced SDS-PAGE gel image is displayed in the upper panel. Quantitative analysis by ImageJ software of the SDS-PAGE gel image (lower panel). The intensities of the dimeric TLR7 and monomeric TLR7 band areas were calculated, respectively. A green dashed line indicates the value of dimeric TLR7 in the absence of any ligands. (C) Gel filtration analysis of glutaraldehyde-crosslinked TLR7 in the absence or presence of 1.0 mmol/L TH-407b. The elution time of dimeric and monomeric TLR7 is indicated by black arrows. Solid lines and dashed lines indicate the absorbance unit (AU) at 280 nm (A_{280}) and 260 nm (A_{260}), respectively.

hydrophobic residues (L353, F349, F351, V355, V381, F408, F506*, F507*, and L528*). Y264, N265, Q531*, and S530* form van der Waals interaction with TH-407b backbones at the bottom of the pocket. The quinoline group is sandwiched by F351 and F507* which forms π−π stacking interactions. The nitro group and the N atom in the quinoline group form multiple hydrogen bonds with the main and/or side chain of Y264 and Q354. The carbonyl group on adamantine forms a hydrogen bond with the R553* side chain, possibly explaining the stronger activity of TH-407b than TH-407a. The TLR7 antagonist binding site corresponds to the same position that was previously identified in TLR8[7,8] (Fig. S5C and S5D). Similar features are observed between them, such as hydrophobic environments composed by conserved residues (Fig. S5C and S5D).

3.5. Inhibition of TLR7 through stabilizing the inactivated dimeric state by TH-407b

We conducted another inhibition assay using ITC titration (Fig. 4A). The binding of loxoribine to TLR7 was confirmed with

a binding affinity of $K_D = 4.4$ μmol/L and $\Delta H = -5828$ cal/mol. By contrast, the heat change upon the titration of loxoribine was completely obliterated in the presence of pre-mixed TH-407b. This result demonstrates that the TH-407b-induced inactivated dimeric TLR7 inhibits the formation of activated dimeric TLR7.

We also performed an ITC titration of TH-407b to TLR7 in the presence of an agonist (100 μmol/L loxoribine). Interestingly, even under this condition, we were able to detect the binding of TH-407b to TLR7 with a comparable K_D value (11.7 μmol/L), although the ΔH was largely reduced (Supporting Information Fig. S6). These data indicate the capability of TH-407b binding to and possibly reversing the activated form of TLR7.

Therefore, we proposed a model of TLR7 inhibition by TH-407b (Fig. 4B): Unliganded TLR7 exists majorly as a monomeric form, possibly being in a monomer-dimer equilibrium in a monomer dominant manner due to the rapid dissociation of the dimer. TH-407b shifts the equilibrium toward dimer by inducing and stabilizing an inactivated dimeric TLR7 in which the two C-terminuses are apart from each other and the downstream
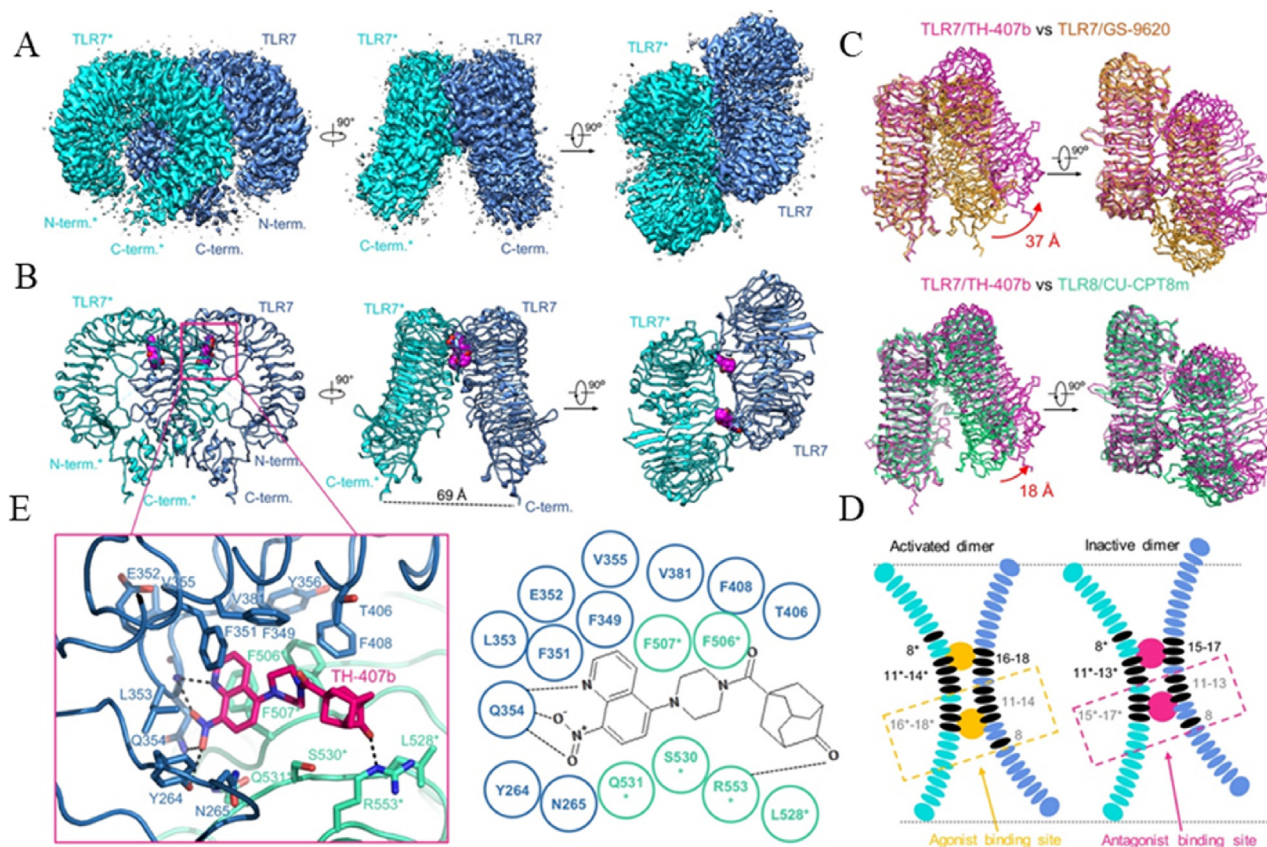
Figure 3 Cryo-EM structure of TLR7/TH-407b complex. (A) Cryo-EM density maps of the TLR7/TH-407b complex are shown as surface representations. The maps are segmented according to different TLR7 protomers and colored by blue and cyan colors, respectively. Three different views (front, side, and top) are displayed. Map levels are countered at 0.032. (B) Cryo-EM structure of the TLR7/TH-407b complex is shown as cartoon (polypeptide) and space-filling (TH-407b) representations. The C, O, and N atoms of TH-407b are colored magenta, red and blue, respectively. The distance (dashed line) between the Cα atoms of the two C-terminal residues in two protomers are indicated. (C) Comparison of the TLR7/TH-407b complex with TLR7/GS9620 complex (PDB: 5ZSJ) (upper) and with TLR8/CU-CPT8m complex (PDB: 5WYX) (lower). Protein structures are shown as ribbon representations. Distances (red dashed lines) between the Cα atoms of the two C-terminal residues in two structures are indicated. (D) Schematic representations of TLR7/agonist complex and TLR7/TH-407b complex structures are shown. LRR domains are displayed by tandem elliptical shapes and ligands are displayed by circles. LRRs involved in ligand binding are colored black and indicated by numbers. (E) Close-up view of TH-407b recognition (Left). Residues within 5 Å of TH-407b are shown in stick representations. A schematic view representing the recognition mode of TH-407b is displayed (right). Dashed lines indicate hydrogen bonds.

cytosolic TIR oligomerization process cannot be initiated. TH-407b upkeeps this inactivated dimer upon agonist engagement and eventually inhibits the immune response.

3.6. Therapeutic potential of small-molecule TLR7 inhibitors in treating SLE

TLR7 is over-expressed in peripheral blood mononuclear cells (PBMCs) of patients with systemic lupus erythematosus (SLE)[4,5], making it a potential target for drug development. In order to validate the therapeutic potential of TH-407b, we measured the level of different cytokines in the patients' primary cells treated by various concentrations of TH-407b. We collected the fresh blood from three SLE patients and their PBMCs were isolated by density gradient centrifugation[24]. Then immediately, cells were treated with indicated compound TH-407b and incubated for 24 h. Finally, through ELISA test, we found that TH-407b could dose-dependently inhibit the production of TNF-α, IL-6, and interleukin-1 beta (IL-1β) in PBMCs harvested from SLE patients (Fig. 5) without any toxicity. Meanwhile, whole

blood from healthy individuals, when stimulated with R848 and subsequently treated with different TH-407b concentrations for 24 h, displayed a significant inhibition of IFN-α and interferon-stimulated genes (ISGs) mRNA levels (Supporting Information Fig. S7).

These results showed that TH-407b treatment exerted potent anti-inflammatory effects in SLE patients, further supporting to previous speculations that TLR7 might play a role in the pathogenesis of these inflammatory disorder and autoimmune diseases.

In order to verify *in vivo* therapeutic potential of TH-407b, *MRL/lpr* mice, a genetically engineered mouse strain prone to SLE was chosen. *MRL/lpr* mice are widely used as a SLE mouse model with comparable symptoms of human patients[25]. We used female *MRL/lpr* mice for about 14 weeks to investigate the pharmacodynamic properties of TH-407b. Since TH-407b has demonstrated a relatively short half-life (Supporting Information Fig. S8), it was administered orally twice daily at a dose of 100 mg/kg. Positive control group was administered hydroxychloroquine (HCQ, a drug widely used to treat SLE) orally once daily at 100 mg/kg, and saline was administered for the placebo group.
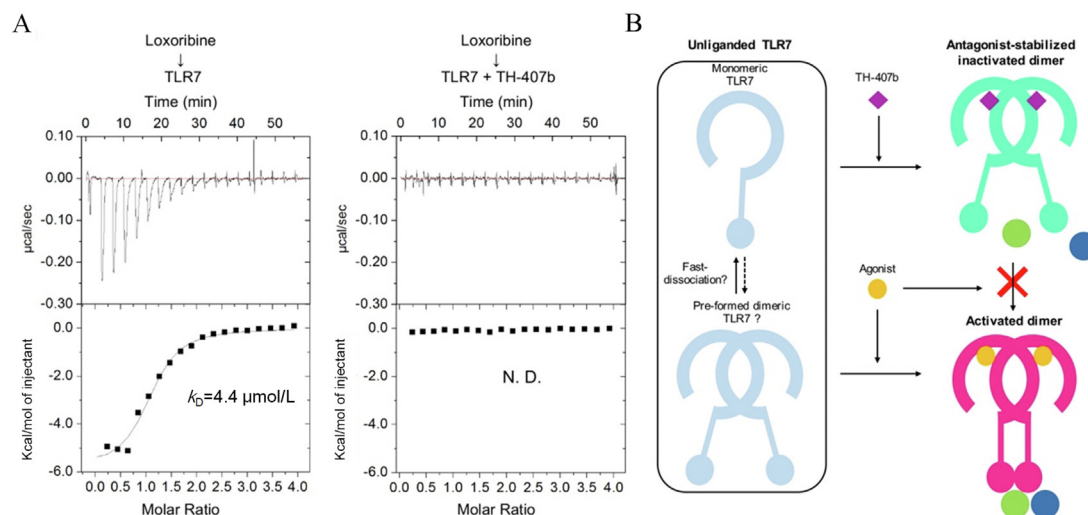
Figure 4 TLR7 inhibition mechanism of TH-407b. (A) ITC titrations of loxoribine into TLR7 recombinant proteins in the absence or presence of 500 μmol/L TH-407b. Dissociation constant value (K_D) and enthalpy change (ΔH) are indicated. N.D. means 'not detected'. (B) Model of TLR7 inhibition by TH-B. Unliganded TLR7 is mainly in monomeric form and might also form a pre-formed dimeric form. TH-407b induces an inactivated dimer of TLR7, which blocks the cytosolic assembly of TIR domains. The formation of activated dimer induced by TLR7 agonists and downstream signal transduction is inhibited by TH-407b.

After 4-week administration, the survival rate of TH-407b group and HCQ group was significantly higher than placebo group (Fig. 6A), and the rate and severity of skin lesions was much lower (Fig. 6B and Supporting Information Fig. S9). After dissection, we found that the spleen and lymph nodes (Supporting Information Fig. S10) of mice in TH-407b group and HCQ group were significantly smaller than placebo group since there is no significant difference in mice weight among three groups (Fig. 6C). Blood was collected each week during administration and ANA, anti-ds-DNA antibodies levels were detected by using ELISA assay. The results showed that placebo group also had significantly higher content than other groups (Fig. 6D). Histological analysis of the kidneys confirmed that TH-407b group exhibited mild glomerulonephritis while placebo group displayed severe glomerulonephritis (Fig. 6E and F). The average diameter of glomeruli in TH-407b group was smaller than placebo group (Fig. 6G).

Importantly, acute toxicology experiments indicated negligible acute toxicity, even at a high dose of 1000 mg/kg. Long-term treatment toxicity assessment demonstrated no significant toxicity with a dose of 100 mg/kg administered twice daily for 4 weeks. Furthermore, an *in vitro* bacterial reverse mutation assay revealed no mutagenic potential for TH-407b (Supporting Information

Table S2). A hERG binding toxicity assessment indicated minimal inhibitory effect on hERG potassium channels, suggesting a low risk of cardiac toxicity (Supporting Information Fig. S11). Taken together, these results indicated that TH-407b could effectively improve the survival rate of MRL/lpr mice and improve their symptoms, which further verified its therapeutic potential in the treatment of SLE.

3.7. Data availability

The cryo-EM density map of the TLR7/TH-407b complex has been deposited in the Electron Microscopy Data Bank (EMDB) under accession code EMD-35258. The coordinate of the TLR7/TH-407b complex structure has been deposited in the RCSB Protein Data Bank (PDB) under accession code 8I96.

4. Discussion

TLR7 and TLR8 are closely related TLRs with common activation mechanisms. A large number of TLR8 antagonists and their complex structures have already been reported[7,8] but few small-molecule inhibitors with elaborated inhibition mechanism
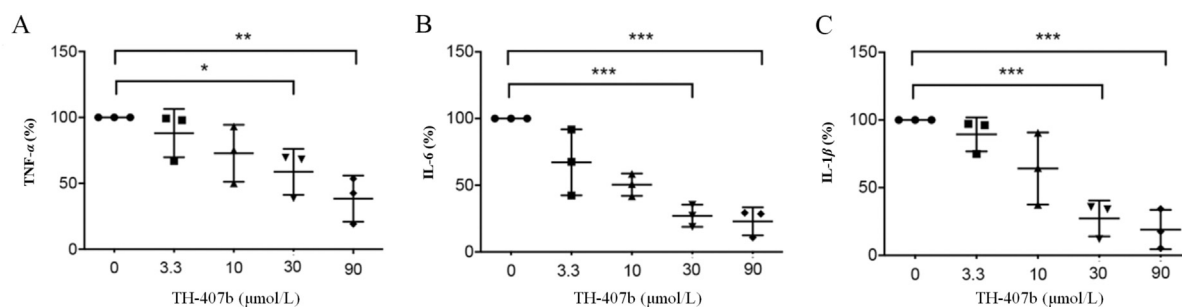

Figure 5 The potential for medicine of TH-407b. (A, B, C) TH-407b could dose-dependently inhibit the production of TNF-α, IL-6, and IL-1β in PBMCs harvested from the SLE patients. Each data point represents an independent sample read. (Center lines indicate means, and whiskers indicate $\pm$ SEM. P values were determined using one-way ANOVA; *$P < 0.05$, **$P < 0.01$, ***$P < 0.001$).
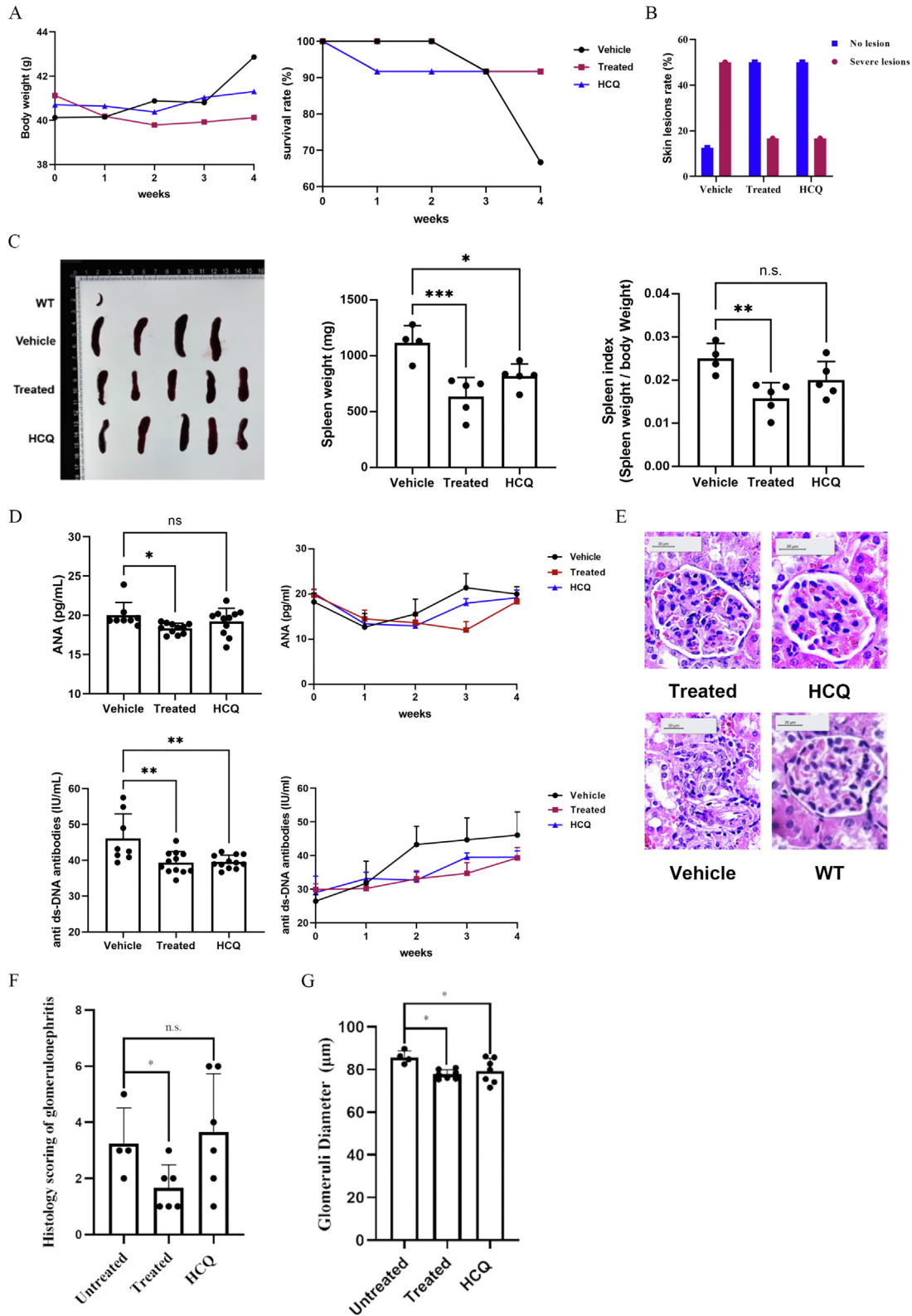
Figure 6 Efficacy of TH-407b in treating MRL/lpr mice. (A) Body weight and survival rate. (B) Skin lesions. (C) Spleen weight. (D) Mice ANA & anti-ds-DNA antibodies level. (E) Histopathological images of the glomeruli with HE stain. (F) Histology scoring for the extent of glomerulonephritis. The scale bar represents 20 μm. (G) Average diameter of glomeruli. Center lines indicate means, and whiskers indicate ±SEM. P values were determined using one-way ANOVA; $*P < 0.05$, $**P < 0.01$, $***P < 0.001$.

have been reported for TLR7. Here, we reported a well-characterized small-molecule inhibitor TH-407b to TLR7 with improved potency and selectivity in cultured cell lines and *ex vivo* specimens from SLE patients. In addition, TH-407b showed good efficacy in treating SLE in mice, which not only demonstrates it presents considerable therapeutic potential, but also indicates that TLR7 might play a role in this inflammatory disorder and autoimmune diseases like SLE. In particular, the complex structure of TLR7 bound to its specific inhibitor TH-407b resolved by cryo-EM analysis revealed the detailed molecular mechanism that TH-407b stabilized the resting/inactivated state of TLR7 and interrupted the TLR7-mediated signaling cascades. As an atomistic resolution cryo-EM structure of the TLR family, it not only of value to facilitate structure-based drug design, but also shed light to methodology development of small proteins using EM.

The recognition of backbones of TH-407b and CU-CPT8m *via* characteristic $\pi-\pi$ stacking interactions (TLR7: F351, F349, F507*; TLR8: Y348, F346, F495*) are similar. Nonetheless, detailed local structures of the two binding pockets still differ largely from each other, which shapes their unique ligand preference. TLR7 has a more spacious pocket with an entrance composed of F408, F506*, L528*, R553*. By contrast, the binding pocket of TLR8 is more compact and is completely encapsulated with no entrance existing. Actually, molecular weights of published TLR8-specific antagonists targeting this binding pocket are relatively smaller compared to TH-407b[7,8]. Moreover, Q354 of TLR7 forms hydrogen bond interactions with TH-407b *via* both its main chain and side chain. The corresponding residue in TLR8 is G351, which is not conserved. The different pocket sizes and different patterns of hydrogen bond interactions are possible factors that defines their ligand preference.

To assess the *in vivo* therapeutic potential of the TLR8-selective compound, female MRL/lpr mice were utilized in a 14-week study, investigating the pharmacodynamic properties of **S14**. Administered orally once daily at a dose of 50 mg/kg, **S14** displayed no significant alterations in spleen index, skin lesion severity, glomerular diameter, or ANA and anti-ds-DNA antibody levels compared to the placebo group. Intriguingly, the survival rate of the **S14** group was notably lower than the placebo group (Supporting Information Fig. S12). These findings indicate the ineffectiveness of the TLR8-selective compound in SLE treatment, thereby reinforcing the distinct functional roles of TLR7 and TLR8. In summary, we reported by a combination of structural, chemical biology, and cellular approaches for TLR7, locking its resting state could be a novel strategy for the SLE treatment.

Acknowledgments

Author contributions

Hang Yin conceived the project. Meng Wang, Hekai Chen, Tuan Zhang, Zhikuan Zhang, Shuangshuang Jiang, Umeharu Ohto, Jing Li, Toshiyuki Shimizu, and Hang Yin designed all experiments. Hang Yin, Hekai Chen, and Shuangshuang Jiang are responsible for inhibitor development. Hekai Chen, Xuwen Xiang, Meng Gao, Shuangshuang Jiang, Kejun Yin, and Tuan Zhang are responsible for chemical synthesis and characterizations. Meng Wang, Hekai Chen, Zhikuan Zhang, Yilan Guo, Shuangshuang Jiang, Jing Li, and Mintao Chen performed all biochemical assays. Zhikuan Zhang and Umeharu Ohto performed protein expression, cross-linking assay, ITC titration and structural determination. Meng Wang, Tuan Zhang and Xincheng Zhong performed animal experiment. All authors analyzed the data. Meng Wang, Hang Yin, Toshiyuki Shimizu, Hekai Chen, Tuan Zhang, Zhikuan Zhang, Meng Gao, Yilan Guo, Shuangshuang Jiang, Umeharu Ohto, and Jian Huang prepared the manuscript.

Conflicts of interest

Hang Yin, Shuangshuang Jiang, and Hekai Chen have filed a patent application based on the technology reported in this manuscript.

Appendix A.   Supporting information

Supporting information to this article can be found online at https://doi.org/10.1016/j.apsb.2024.08.016.

References

1. Kawai T, Akira S. The role of pattern-recognition receptors in innate immunity: update on Toll-like receptors. *Nat Immunol* 2010;**11**: 373−84.
2. O'Neill LA, Golenbock D, Bowie AG. The history of Toll-like receptors−redefining innate immunity. *Nat Rev Immunol* 2013;**13**: 453−60.
3. Goh FG, Midwood KS. Intrinsic danger: activation of Toll-like receptors in rheumatoid arthritis. *Rheumatol* 2012;**51**:7−23.
4. Nickerson KM, Christensen SR, Shupe J, Kashgarian M, Kim D, Elkon K, et al. TLR9 regulates TLR7- and MyD88-dependent autoantibody production and disease in a murine model of lupus. *J Immunol* 2010;**184**:1840−8.
5. Clancy RM, Markham AJ, Buyon JP. Endosomal Toll-like receptors in clinically overt and silent autoimmunity. *Immunol Rev* 2016;**269**: 76−84.
6. Yin H, Flynn AD. Drugging membrane protein interactions. *Annu Rev Biomed Eng* 2016;**18**:51−76.
7. Hu Z, Tanji H, Jiang S, Zhang S, Koo K, Chan J, et al. Small-molecule TLR8 antagonists *via* structure-based rational design. *Cell Chem Biol* 2018;**25**:1286−91.e3.
8. Zhang S, Hu Z, Tanji H, Jiang S, Das N, Li J, et al. Small-molecule inhibition of TLR8 through stabilization of its resting state. *Nat Chem Biol* 2018;**14**:58−64.
9. Jiang S, Tanji H, Yin K, Zhang S, Sakaniwa K, Huang J, et al. Rationally designed small-molecule inhibitors targeting an unconventional pocket on the TLR8 protein−protein interface. *J Med Chem* 2020;**63**:4117−32.
10. Bou Karroum N, Moarbess G, Guichou JF, Bonnet PA, Patinote C, Bouharoun-Tayoun H, et al. Novel and selective TLR7 antagonists among the imidazo[1,2-*a*]pyrazines, imidazo[1,5-*a*]quinoxalines, and pyrazolo[1,5-*a*]quinoxalines series. *J Med Chem* 2019;**62**:7015−31.
11. Mukherjee A, Raychaudhuri D, Sinha BP, Kundu B, Mitra M, Paul B, et al. A chemical switch for transforming a purine agonist for Toll-like receptor 7 to a clinically relevant antagonist. *J Med Chem* 2020;**63**:4776−89.
12. Manson JJ, Rahman A. Systemic lupus erythematosus. *Orphanet J Rare Dis* 2006;**1**:6.
13. Rahman A, Isenberg DA. Systemic lupus erythematosus. *N Engl J Med* 2008;**358**:929−39.

14. Pisitkun P, Deane JA, Difilippantonio MJ, Tarasenko T, Satterthwaite AB, Bolland S. Autoreactive B cell responses to RNA-related antigens due to TLR7 gene duplication. *Science* 2006;**312**:1669−72.

15. Deane JA, Pisitkun P, Barrett RS, Feigenbaum L, Town T, Ward JM, et al. Control of toll-like receptor 7 expression is essential to restrict autoimmunity and dendritic cell proliferation. *Immunity* 2007;**27**:801−10.

16. Fairhurst AM, Hwang SH, Wang A, Tian XH, Boudreaux C, Zhou XJ, et al. Yaa autoimmune phenotypes are conferred by overexpression of TLR7. *Eur J Immunol* 2008;**38**:1971−8.

17. Souyris M, Cenac C, Azar P, Daviaud D, Canivet A, Grunenwald S, et al. TLR7 escapes X chromosome inactivation in immune cells. *Sci Immunol* 2018;**3**:eaap8855.

18. Klopp-Schulze L, Shaw JV, Dong JQ, Khandelwal A, Vazquez-Mateo C, Goteti K. Applying modeling and simulations for rational dose selection of novel Toll-like receptor 7/8 Inhibitor enpatoran for indications of high medical need. *Clin Pharmacol Ther* 2022;**112**:297−306.

19. Tojo S, Zhang Z, Matsui H, Tahara M, Ikeguchi M, Kochi M, et al. Structural analysis reveals TLR7 dynamics underlying antagonism. *Nat Commun* 2020;**11**:5204.

20. Kawai T, Akira S. Signaling to NF-kappaB by toll-like receptors. *Trends Mol Med* 2007;**13**:460−9.

21. Zhang Z, Ohto U, Shibata T, Krayukhina E, Taoka M, Yamauchi Y, et al. Structural analysis reveals that Toll-like receptor 7 is a dual receptor for guanosine and single-stranded RNA. *Immunity* 2016;**45**:737−48.

22. Tanji H, Ohto U, Shibata T, Miyake K, Shimizu T. Structural reorganization of the Toll-like receptor 8 dimer induced by agonistic ligands. *Science* 2013;**339**:1426−9.

23. Zhang Z, Ohto U, Shibata T, Taoka M, Yamauchi Y, Sato R, et al. Structural analyses of Toll-like receptor 7 reveal detailed RNA sequence specificity and recognition mechanism of agonistic ligands. *Cell Rep* 2018;**25**:3371−81.e5.

24. Ulmer AJ, Scholz W, Ernst M, Brandt E, Flad HD. Isolation and subfractionation of human peripheral blood mononuclear cells (PBMC) by density gradient centrifugation on Percoll. *Immunobiology* 1984;**166**:238−50.

25. Rottman JB, Willis CR. Mouse models of systemic lupus erythematosus reveal a complex pathogenesis. *Vet Pathol* 2010;**47**:664−76.

26. Mastronarde DN. Automated electron microscope tomography using robust prediction of specimen movements. *J Struct Biol* 2005;**152**:36−51.

27. Zivanov J, Nakane T, Forsberg BO, Kimanius D, Hagen WJ, Lindahl E, et al. New tools for automated high-resolution cryo-EM structure determination in RELION-3. *Elife* 2018;**7**:4586.

28. Zheng SQ, Palovcak E, Armache JP, Verba KA, Cheng Y, Agard DA. MotionCor2: anisotropic correction of beam-induced motion for improved cryo-electron microscopy. *Nat Methods* 2017;**14**:331−2.

29. Rohou A, Grigorieff N. CTFFIND4: fast and accurate defocus estimation from electron micrographs. *J Struct Biol* 2015;**192**:216−21.

30. Kucukelbir A, Sigworth FJ, Tagare HD. Quantifying the local resolution of cryo-EM density maps. *Nat Methods* 2014;**11**:63−5.

31. Adams PD, Afonine PV, Bunkoczi G, Chen VB, Davis IW, Echols N, et al. PHENIX: a comprehensive Python-based system for macromolecular structure solution. *Acta Crystallogr D Biol Crystallogr* 2010;**66**:213−21.

32. Emsley P, Cowtan K. Coot: model-building tools for molecular graphics. *Acta Crystallogr D Biol Crystallogr* 2004;**60**:2126−32.

33. Goddard TD, Huang CC, Meng EC, Pettersen EF, Couch GS, Morris JH, et al. UCSF ChimeraX: meeting modern challenges in visualization and analysis. *Protein Sci* 2018;**27**:14−25.